

Citation for published version:
Ellingford, C, Zhang, R, Wemyss, AM, Zhang, Y, Brown, OB, Zhou, H, Keogh, P, Bowen, C & Wan, C 2020, 'Self-healing dielectric elastomers for damage-Tolerant actuation and energy harvesting', ACS Applied Materials and Interfaces, vol. 12, no. 6, pp. 7595-7604. https://doi.org/10.1021/acsami.9b21957

DOI:

10.1021/acsami.9b21957

Publication date: 2020

Document Version Peer reviewed version

Link to publication

This document is the Accepted Manuscript version of a Published Work that appeared in final form in ACS Appl. Mater. Interfaces, copyright @ American Chemical Society after peer review and technical editing by the publisher. To access the final edited and published work see https://pubs.acs.org/doi/10.1021/acsami.9b21957

University of Bath

Alternative formats

If you require this document in an alternative format, please contact: openaccess@bath.ac.uk

Copyright and moral rights for the publications made accessible in the public portal are retained by the authors and/or other copyright owners and it is a condition of accessing publications that users recognise and abide by the legal requirements associated with these rights.

Take down policyIf you believe that this document breaches copyright please contact us providing details, and we will remove access to the work immediately and investigate your claim.

Download date: 07 Mar 2023

Self-healing Dielectric Elastomers for Damage Tolerant Actuation and Energy Harvesting

Christopher Ellingford¹, Runan Zhang², Alan M. Wemyss¹, Yan Zhang², Oliver B.Brown¹, Hongzhao Zhou², Patrick Keogh², Christopher Bowen^{2*}, Chaoying Wan^{1*}

¹ International Institute for Nanocomposites Manufacturing (IINM), WMG, University of Warwick, CV4 7AL, UK

² Department of Mechanical Engineering, University of Bath, BA2 7AY, UK

Christopher Ellingford, Oliver B. Brown, Dr. Alan M. Wemyss, Dr. Chaoying Wan* International Institute for Nanocomposites Manufacturing (IINM), WMG, University of Warwick, CV4 7AL, UK

Email: Chaoying.wan@warwick.ac.uk

Runan Zhang, Yan Zhang, Hongzhao Zhou, Prof. Patrick Keogh, Prof. Christopher Bowen Department of Mechanical Engineering, University of Bath, BA2 2ET, UK

Email: msscrb@bath.ac.uk; chaoying.wan@warwick.ac.uk

Key Words: Dielectric Elastomer, Actuation, Energy Harvesting, Intrinsic Self-healing, Dielectric Breakdown Strength, Relative Permittivity

Abstract

The actuation and energy harvesting performance of dielectric elastomers are strongly related to their intrinsic electrical and mechanical properties. For future resilient smart transducers, a fast actuation response, efficient energy harvesting performance and mechanical robustness are key requirements. In this work, we demonstrate that poly (styrene-butadiene-styrene) (SBS) can be converted into a self-healing dielectric elastomer with high permittivity and low dielectric loss which can be deformed to large mechanical strains; these are key requirements for actuation and energy harvesting applications. Using a one-step click reaction at room

temperature for 20 mins, methyl-3-mercaptoproionate (M3M) was grafted to SBS and reached 95.2% of grafting ratios. The resultant M3M-SBS can be deformed to a high mechanical strain of 1000%, with a relative permittivity of $\varepsilon_r = 7.5$ and a low tan $\delta = 0.03$. When used in a dielectric actuator it can provide 9.2% strain at an electric field of 39.5 MV m⁻¹, and can also generate energy density of 11 mJ g⁻¹ from energy harvesting. After being subjected to mechanical damage, the self-healed elastomer can recover 44% of its breakdown strength during energy harvesting. This work demonstrates a facile route to produce self-healing, high permittivity and low dielectric loss elastomers for both actuation and energy harvesting, which is applicable to a wide range of diene elastomer systems.

Introduction

Smart and high performance actuation and energy harvesting devices based on dielectric elastomers are highly dependent on the electrical and mechanical properties of the material used to create them. For example, a high relative permittivity ε_r , and low dielectric loss ε "are required to ensure efficient energy transduction. With regard to mechanical properties, a high tensile strength, low Young's modulus and high elastic strain are needed to provide a resilient material capable of large elastic deformations during both actuation and energy harvesting. Operationally, a high breakdown strength is essential to maximise the operating voltage and prevent electrically induced failures.

To aid in the selection of materials for energy actuation or harvesting, appropriate *Figures of Merit (FoM)* that combine the key materials properties can be used to estimate performance for the two applications. These are,

$$FoM_{harvesting} = \varepsilon_0 \varepsilon_r E_b^2 \tag{1}$$

$$FoM_{actuation} = \frac{3\varepsilon_0 \varepsilon_r E_b^2}{\gamma} \tag{2}$$

where ε_0 is vacuum permittivity, E_b is breakdown strength and Y is the Young's modulus.¹ Equation 1 shows that a breakdown strength and relative permittivity are key properties to create a successful polymer for energy harvesting, whilst for actuation, the Young's modulus is also a key factor, see Equation 2, since a low modulus leads to a greater deformation in response to an applied electric field. In addition, the ability to provide a large *elastic* deformation during operation is highly desirable since during actuation or energy harvesting the material is subjected to repeated recoverable deformation.

However, over a prolonged cycle lifetime, polymers can undergo irreversible mechanical and electrical induced failure. The creation of self-healing elastomers is an emerging technology to improve the operational stability and service lifetimes of such dielectric devices. Self-healing polymers can be designed by introducing reversible covalent or non-covalent bonds into the polymer chains. The use of dynamic covalent bonds, such as diels-alder interactions disulphide or imine bonds I0-11 allows the polymer chains to break and reform during thermal treatment. The introduction of supramolecular interactions, such as hydrogen bonding I2-14, ionic bonding I5, π - π stacking I6-17 or metal-ligand coordination I8-19, into polymer structures can also assist the self-healing process, due to the reversible and reformative nature of the non-covalent interactions. The bond strength of the non-covalent interactions affect the self-healing dynamics and kinetics, where supramolecular interactions are also affected by phase segregation, crystallisation and chain entanglement Interactions are also affected by phase segregation, crystallisation and chain entanglement Polymers, with the potential to make an impact on sustainable industry and our environment by creating devices which are able to recover properties after the introduction of damage.

Self-healing dielectric elastomers has primarily been achieved using silicone elastomers. Recent examples include Sun *et al.* forming a blend of silicone chains grafted with carboxy and amine groups which form hydrogen bonds between the polymer chains. Self-healing at

80 °C for 5 hours led to a 115% recovery in tensile strength due to hydrogen bond reformation. However, when self-healed at 100 °C, the hydrogen bonds were converted to ionic bonds, increasing the breakdown strength of the elastomer. The relative permittivity of the modified dielectric elastomer increased to $\varepsilon_r \approx 4.4$, and actuated up to 8.3% at 15 kV mm⁻¹.²¹ Another example incorporated an interpenetrating silicone polymer network and an ionic silicone species by Madsen *et al.* obtaining up to 77% strain recovery with a healed strain at break of 300%. However, the healing time was long and healing of the samples required 120 °C for 12 hours. Nonetheless, the relative permittivity of the system increased to $\varepsilon_r \approx 4.3$ and a high breakdown strength of 57 V μ m⁻¹ was obtained.²²

However, not all modifications lead to a self-healing nature. Dünki *et al.* modified poly(methylvinylsiloxane) with sulphonyl groups via thiol-ene click chemistry and enhanced the relative permittivity up to $\varepsilon_r \sim 22.7$ at 10^4 Hz, albeit accompanied by a high tan δ loss of >0.25. 23 The hydrosilylation of silicone elastomers with allyl cyanide polar groups increased the relative permittivity of silicone to $\varepsilon_r \sim 15.9$ at 10^3 Hz. 24 Furthermore, the grafting of electrically conducting groups, such as copper phthalocyanine (CuPc) to poly(urethane), successfully enhanced the relative permittivity up to $\varepsilon_r \sim 30$ at 10^3 Hz whilst maintaining a low tan δ . Moreover grafting a conducting poly(aniline) polymer to the CuPc ring increased the permittivity to $\varepsilon_r \sim 105$ at 10^3 Hz. 25 due to the formation of microcapacitors in the insulating polymer matrix. Whilst the permittivity of such materials is often reported, the breakdown strength is less studied, despite its important role in the figures of merit for both actuation (Equation 1) and energy harvesting (Equation 2); this may be due to the more complex process associated with dielectric strength characterisation.

In addition to the self-healing properties, the electromechanical properties of dielectric elastomers can also be tailored by the choice of polar pedant groups and the grafting densities¹, ²⁶⁻²⁷. A fascinating synergy is that the inclusion of appropriate pedant groups can enhance the

intra- and inter-molecular interactions among the polymer chains which can benefit self-healing, increase strain, reduce stiffness and increase energy transduction functions for producing robust and high performance dielectric actuators and harvesters. Poly (styrene-butadiene-styrene), SBS, is a commercial thermoplastic elastomer with favourable mechanical properties and good melt-processing ability, but is not inherently self-healable. In this work, we modify SBS via a one-step thiol-ene click chemistry with methyl-3-mercaptopropionate (M3M), as illustrated in Figure S1. The effect of the grafted polar group on the mechanical, electrical and self-healing properties of the elastomer are investigated in detail. The densely grafted polar M3M side chains offer the potential to increase the polarity of SBS, hence enhancing the dielectric permittivity. Meanwhile, the linear side chain decreases the polymer chain entanglement of the elastomer and compatibilises the phase separation of SBS, which also benefits the mechanical strain and self-healing function. Dielectric actuator and energy harvesting devices are constructed to examine their ability to self-heal and continue to operate after the introduction of damage.

Results and Discussion

The modification of SBS with methyl-3-mercaptopropionate (M3M) resulted in the formation of a M3M-SBS elastomer with a molar grafting ratio of 95.2%, and this has been characterised by NMR and FTIR in Figure 1. The ¹H NMR in Figure 1a showed that the characteristic alkene peak for SBS at 5.4 ppm disappeared after the reaction. In turn, a CH₃ peak at 3.7~3.8 ppm appeared for MG-SBS for the terminus of the grafted ester. Due to the carbon chain between the thiol and ester of methyl-mercaptopropionate, two triplet peaks at 2.8 and 2.6 ppm were observed for M3M-SBS and these are attributed to the CH₂ closest to the sulphur atom and the CH₂ group closest to the ester group respectively.

Fourier transform infrared spectroscopy (FTIR) in Figure 1b shows that after the grafting reaction, the characteristic alkene groups stretch of SBS disappear, and new peaks associated with the ester appear in the M3M-SBS. Specifically, the alkene group at 3006 cm⁻¹ for SBS disappears after the reaction, whilst a new C=O peak forms at 1733 cm⁻¹ in M3M-SBS. Two symmetric C-O-C stretches appear for M3M-SBS at 979 and 1018 cm⁻¹, demonstrating that the longer carbon chain of methyl-3-mercaptopropionate has an extra mode of vibration. Additionally, the asymmetric C-O-C stretch is observed as two stretches for the M3M-SBS material at 1169 and 1243 cm⁻¹, which overlap with a CH₃ and CH₂ bend at 1195 cm⁻¹ and 1145 cm⁻¹ respectively. Overall, ¹H NMR and FTIR confirms the successful grafting of methyl-3-mercaptopropionate to SBS to form M3M-SBS, with the proposed reaction scheme shown in Figure S1.

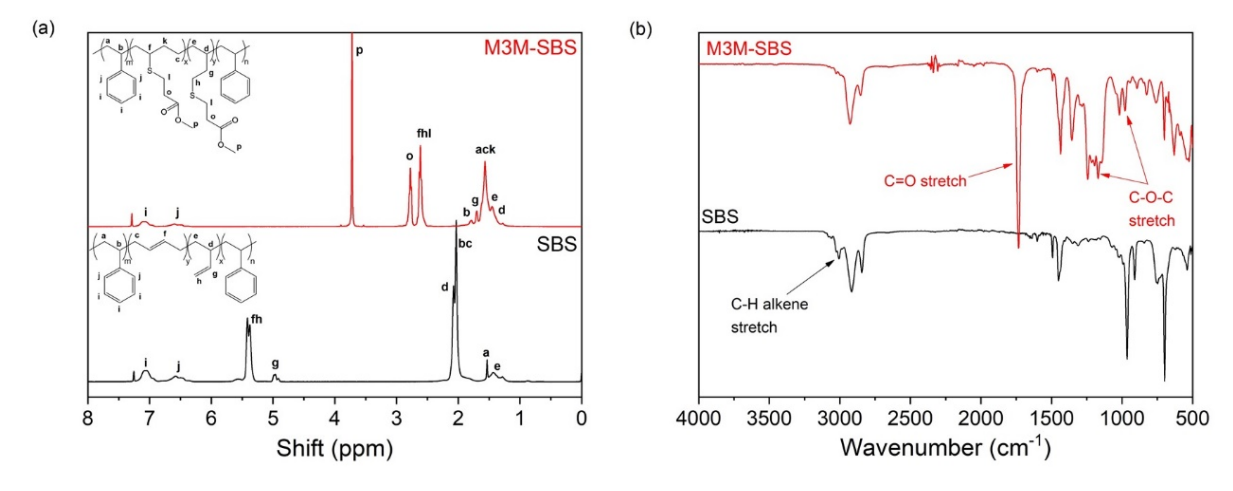


Figure 1 (a) ¹H NMR spectroscopy of SBS and M3M-SBS with assigned peaks. (b) FTIR spectroscopy of SBS and M3M-SBS with peaks of key interested highlighted

Mechanical and Electrical properties. The effects of methyl-3-mercaptopropionate on the mechanical and electrical properties of SBS by the formation of M3M-SBS, as compared with unmodified SBS, are shown in Figure 2 and Table 1 and are now discussed. When compared to SBS, the tensile strength of M3M-SBS decreased from 8.92 MPa to 4.68 MPa, the Young's

modulus decreased from 51.7 MPa to 2.45 MPa, whilst the elongation at break was enhanced from 857% to 1000%. The reduction in the tensile strength and Young's modulus is due to the change in the polymer chain structure, where the polar group of methyl-3-mercaptopropionate hinders polymer chain entanglement. However, the increased strain at break is a result of the electrostatic interaction of long side chain polar groups preventing failure of the elastomer, see Figure 2a. Over the course of five 100% strain cycles, as shown in Figure S2, the M3M-SBS had a hysteresis loss of less than 20%, significantly lower than SBS (39%). When the strain cycles was increased to 500%, the hysteresis loss of M3M-SBS was 27.7%, significantly lower than that of SBS which was 64.8%. In all elongations, SBS displayed a large hysteresis loop on the first cycle, with the loss reducing by the fifth cycle; see Figure 2b. For M3M-SBS, the loss between the cycles were less, and behaviour of M3M-SBS was more consistent. The difference in stress softening was attributed to the viscoelastic behaviour of the elastomers where the intrinsic modification to create M3M-SBS increased the elastic region of the elastomer, and reduced the viscous region compared to SBS due to the electrostatic interaction between the methyl-3-mercaptopropionate groups and styrene. A reduced hysteresis would be beneficial for both actuation and energy harvesting applications in terms of both reduced loss and consistency in performance. During stress relaxation testing shown in Figure 2c, the equilibrium stress of SBS and M3M-SBS was 40% and 35% lower than their maximum stress, respectively. The lower reduction of the equilibrium stress of M3M-SBS indicates the stronger inter-chain interaction preventing the polymer chains from slipping over each other.

With regard to the electrical properties, the grafted M3M groups led to an increase in the relative permittivity (ε_r) to $\varepsilon_r \sim 7.5$ at 10^3 Hz in Figure 2d, compared to $\varepsilon_r \sim 2.8$ for SBS, while maintaining a low $\tan \delta \sim 0.03$ (where $\tan \delta$ = dielectric loss/relative permittivity), see Figure 2e. The increase in the relative permittivity is attributed to the polarity of the grafted polar group increasing the capacitance of the elastomer. There is an increase in the frequency

dependent response of the permittivity at low frequency for M3M-SBS due to the influence of conductivity, which is indicated by a higher $tan \delta$ loss as compared to SBS at the lower frequency range. This is typically associated with electrode polarisation rather than the actual electrical response of the polymer. This response is also observed in the phase angle for M3M-SBS whereby electrode polarisation causes the polymer to deviate away from -90°, see Figure 2f. A second deviation from -90° in the phase angle is observed above 10^5 Hz, attributed to a relaxation peak caused by the polymer unable to respond to the alternating electric field. This is likely caused by the size of the grafted polar group as the relaxation peak is not observed in SBS. The relaxation peak is also observed in $tan \delta$ at frequencies above 10^5 Hz. AC conductivity of SBS and M3M-SBS is shown in Figure S3. Table 1 shows a comparison of M3M-SBS as a high permittivity, low loss material compared to the unmodified SBS and also compared to the current state of the art in the literature for both SBS and silicone elastomers, and demonstrates the potential improvement of M3M-SBS for actuation and energy harvesting as a result of the significantly improved figures of merit for both applications.

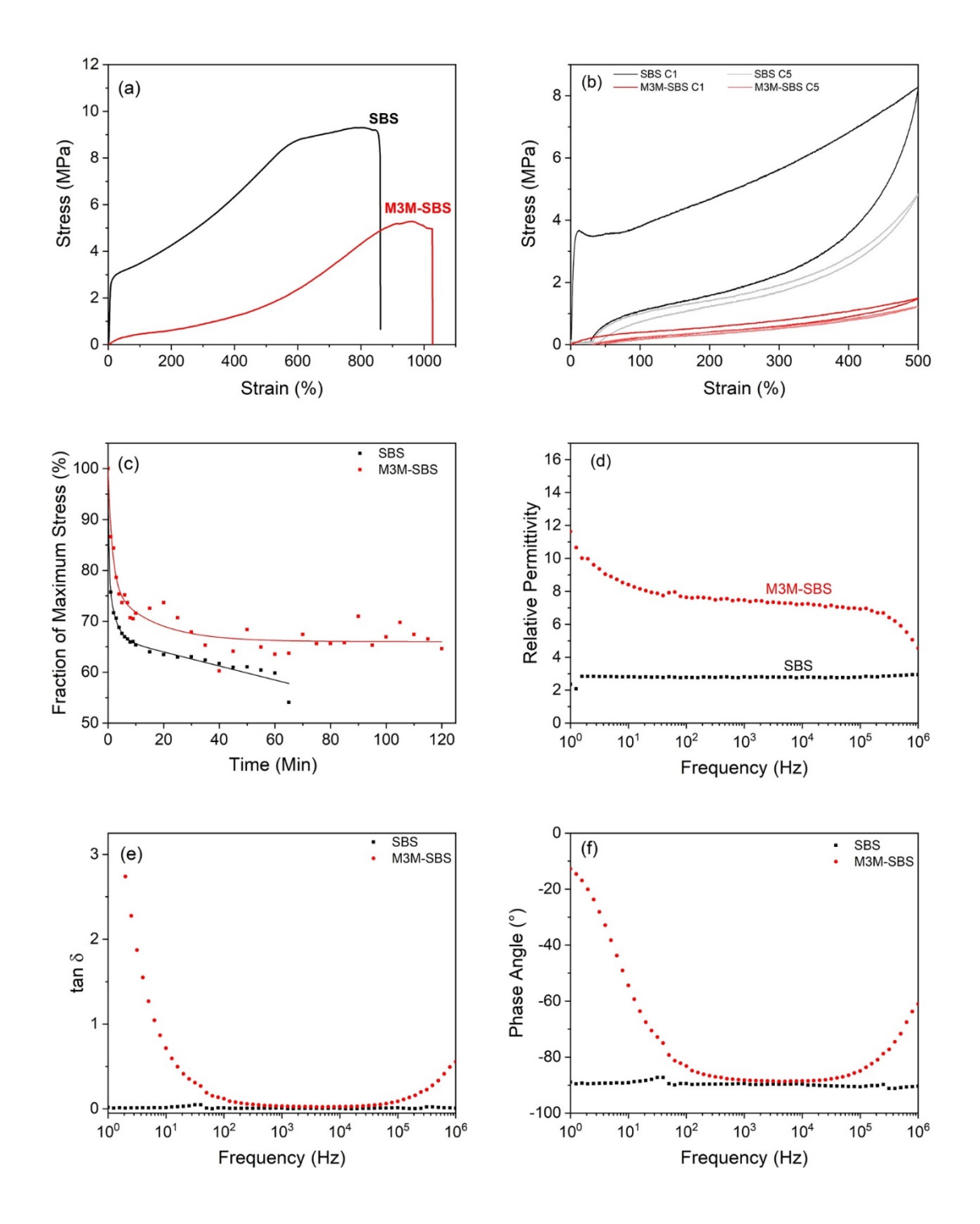


Figure 2 Mechanical and electrical properties of SBS and M3M-SBS: (a) Stress-strain curves, (b) First (C1) and fifth (C5) cycle of cyclic stress softening loops and hysteresis energy loss, (c) Fraction of maximum stress from stress relaxation over time; Impedance spectroscopy showing (d) the relative permittivity, (e) $tan \delta$ and (f) phase angle versus frequency

Table 1 Comparison of mechanical and electrical properties and appropriate Figure of Merit (FoM) values for actuation and energy harvesting for SBS, M3M-SBS and the state of the art in the literature from SBS and Silicone elastomers. FoM values of the modified materials are normalised with respect to SBS for comparison.

| | Elastomer | | | | | |
|---|-----------------------|-------------------------------|-------------------------------|---------------------------|---|--|
| Properties | SBS (this work) | M3M- SBS (this work) | MG- SBS ²⁶ | TGA- SBS ²⁸ | Thioacetic acid modified silicone elastomer ²⁹ | Thiourea modified silicone elastomer ³⁰ |
| Young's modulus (MPa) | 51.7 | 2.4 | 2.9 | 3.3 | 0.12 | 0.79 |
| Elongation at break (%) | 857 | 1000 | 569 | 285 | 252 | 30 |
| Elongation at break after self- healing (%) | Not self- healable | 230 at RT for 3 days | 117 at RT for 3 days | - | - | - |
| Elongation recovery (%) | - | 27 | 21 | - | - | - |
| Stress relaxation (%) | 55 | 65 | 78 | - | - | - |
| Relative permittivity at 1kHz | 2.8 | 7.5 | 11.4 | 7.2 | 4.6 | 18 |
| E _b (MV m ⁻¹) | 20 | 39.6 | 29.8 | 16 | 21.5 | 22.7 |
| FoMactuation | 1.0 | 226.2 | 161.1 | 25.5 | 97.7 | 545.4 |
| FoMharvesting | 1.0 | 10.5 | 9.0 | 1.6 | 1.9 | 8.3 |

Self-healing properties. The self-healing evaluation of M3M-SBS elastomer was performed over a three-day period, shown in Figure S4. Self-healing took place by simply reconnecting two pieces of M3M-SBS, with no external stimulus required. After 3 days of self-healing at room temperature, M3M-SBS exhibited a strain at break of 234%, which is 27% of the strain at break recovery.

The inter-chain interactions in M3M-SBS was monitored by temperature-dependent FTIR to verify the breaking and reforming of the reversible bonding among the polymer chains. The key peaks are shown in Figure 3. Upon heating, the ester C=O peak of methyl-3-mercaptopropionate in M3M-SBS increases by 4 cm⁻¹ from 1734 cm⁻¹ and 6 cm⁻¹ from 1730 cm⁻¹ respectively as the temperature is increased from 30 °C to 150 °C, see Figure 3a. In Figure 3b, the strong peak at 1356 cm⁻¹ is attributed to the bend of the CH₃ in the ester of methyl-3-mercaptopropionate. Upon heating, the peak shifts and broadens as the electrostatic interaction is overcome. This shows that the CH₃ of the ester in M3M-SBS, plays an active role in the interchain electrostatic interaction for self-healing. Finally, in Figure 3c, the peak at 1243 cm⁻¹ shows that the asymmetric C-O-C stretch shifts to a lower wavenumber upon heating. This shift also demonstrates that the C-O-C ester bond is affected by the removal of the interchain electrostatic interaction.

In summary, an examination of the temperature-dependent FTIR demonstrates that the reversible self-healing interaction present in M3M-SBS is due to a δ + proton from the ester of methyl-3-mercaptopropionate and methyl thioglycolate electrostatically interacting with the δ -aromatic centre of styrene²⁶. In comparison, SBS did not display such interactions, nor were obvious characteristic peaks present; these are shown in Figure S5.

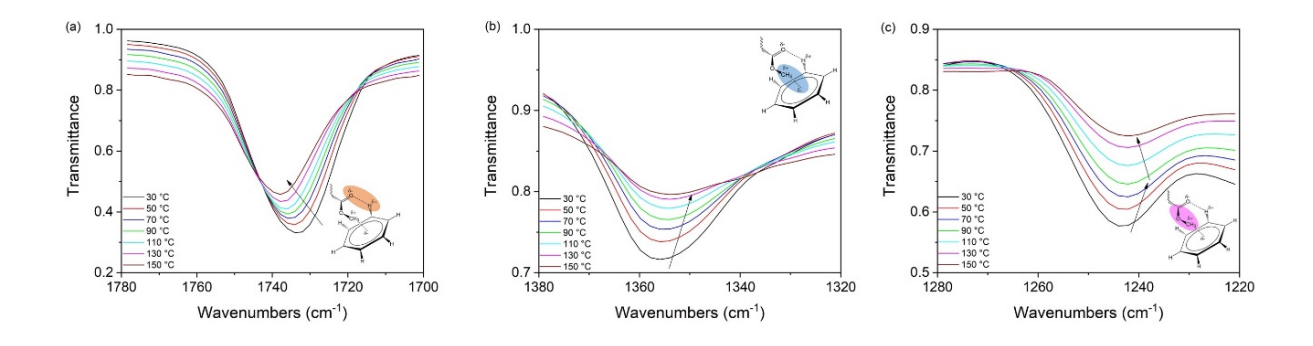


Figure 3 Temperature dependent FTIR for M3M-SBS (a) at 1730 cm⁻¹, (b) at 1356 cm⁻¹ and (c) at 1243 cm⁻¹

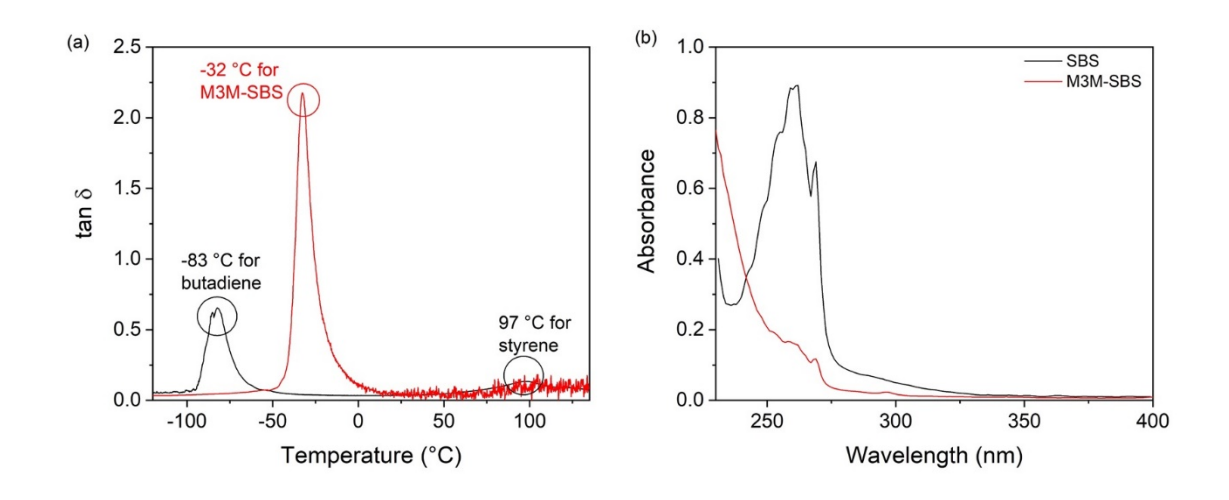


Figure 4 (a) DMTA analysis of mechanical $tan \delta$ in the temperature range of -120 ° to 135 ° and (b) UV-Vis spectroscopy of SBS and M3M-SBS

The inter-chain interaction in the SBS and M3M-SBS elastomers is also detected by DMTA and UV-vis spectroscopy. As shown in Figure 4a, SBS shows two glass transition temperatures (T_g) for butadiene (-83 °C) and styrene (97 °C) blocks. After grafting of methyl-3-mercaptopropionate, a single T_g at -32 °C was detected in M3M-SBS, indicating an enhanced compatibilisation of the butadiene and styrene blocks due to the enhanced polarity of the grafted butadiene blocks. As shown in Figure 4b. For M3M-SBS, a peak attributed to the π - π * transition for the aromatic groups blue shifts from 262 nm for SBS to below the solvent cut-off of 230 nm. This transition occurs in the elastomers due to the δ + proton removing electron

density from the δ - aromatic centre of styrene, increasing the energy required to promote an electron to the π^* orbital in styrene. The length of the polar group attached for M3M-SBS allows greater entanglement of the polymer chains, leading to methyl-3-mercaptopropionate more easily able to interact with styrene and thus a higher energy, lower wavelength of light is required.

Self-healing dielectric elastomer actuation. The actuation and energy harvesting properties of materials are estimated by FoM values¹ according to Equation 1 and 2, and shown in Table 1. According to the FoM equations, the actuation properties of a material depend on the Young's modulus, breakdown strength and relative permittivity. The $FoM_{actuation}$ of M3M-SBS is superior to SBS due to the high permittivity, and low dielectric loss nature of M3M-SBS. Additionally, the $FoM_{actuation}$ is high due to the higher breakdown strength exhibited by M3M-SBS, and its lower Young's modulus compared to SBS.

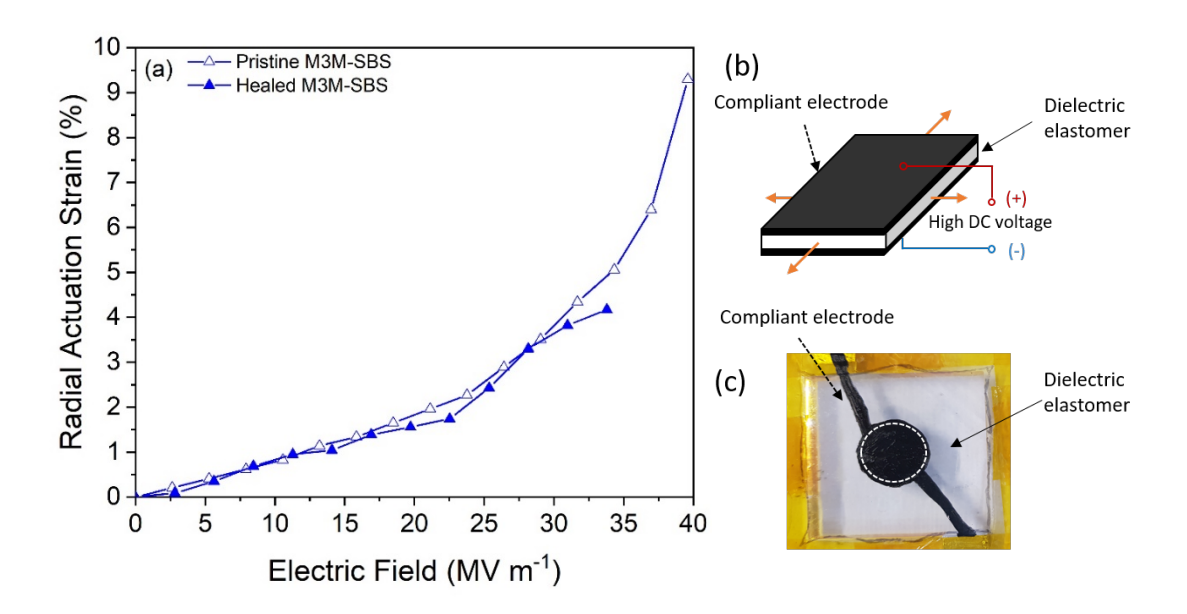


Figure 5 (a) Radial actuation strain of M3M-SBS with electric field for the initial pristine elastomers and healed actuators after the introduction of damage; (b) Schematic of dielectric elastomer actuator, showing the voltage-induced expansion in the planar directions and contraction in thickness; (c) actuation of a modified SBS elastomers at high electric field.

The actuation performance of M3M-SBS in a dielectric actuator before and after self-healing of mechanical damage were investigated. Figure 5a shows measured radial actuation strains of the dielectric actuator devices manufactured from M3M-SBS, before and after self-healing. All samples were pre-strained by 33% equally in planar directions and clamped onto a rigid frame to ensure that voltage-induced deformations occur in-plane, an example is shown in Figure 5 b,c and 7. The applied electric field = $\frac{\Phi}{H}\lambda^2$, is calculated from the driving voltage Φ , the sample thickness H, and the axial pre-strain, λ_p ($\lambda = \lambda_p$). The pristine M3M-SBS generated radial actuation strain up to 9.2% at a maximum electric field of 39.5 MV m⁻¹, while the healed M3M-SBS generated radial actuation strain up to 4.2% at a maximum electric field of 33.5 MV m⁻¹. Comparatively, SBS did not actuate and instead electrically broke down before any signifiant acutuation, primarily due to its higher Young's modulus; see Table 1. Figure 5a shows that the pristine M3M-SBS achieved ~9% radial strain and, when healed, the M3M-SBS actuator recovered 85% of its initial electric breakdown strength and recovered 45% of its strain. The actuation performance of M3M-SBS is similar to the predicted by FoMactuation, suggesting that M3M-SBS would exhibit far superior actuation abilities compared to SBS.

Self-healing dielectric elastomer energy generation. The $FoM_{harvesting}$ data in Table 1 shows that the theoretical energy harvesting and generation abilities of elastomers depend on the electrical breakdown strength and the relative permittivity. The energy harvesting abilities of M3M-SBS before and after self-healing of damage by a mechanical puncture were investigated to determine the durability of the devices; again SBS was not suitable for this application due to its high Young's modulus, see Table 1, which does not allow for the large elastic deformations which are necessary to provide large changes in capacitance for efficient harvesting to be achieved.

A typical constant-voltage energy harvesting circuit is shown in Figure 6a, and the harvesting cycle is shown in Figure 6b which begins in the state A, where a constant DC voltage (1.5kV) is applied to the un-deformed material and electrode by the power supply and diode D1. When pressurized, the capacitance of the elastomer material increases due to an increase in the area and reduction in thickness. The increase in capacitance leads to the device storing more charge at a constant voltage, since Q = CV, until state B is reached at the maximum deformation. During depressurization, the capacitance of the elastomer falls and the voltage across the electrodes is increased since the charge on the electrode remains the same, (i.e. state C in Figure 6b). The charge on the electrode is then collected via diode D2 in Figure 6a at the harvesting voltage (2kV) as the capacitance decreases further (i.e. the state D), before the voltage across the electrodes drops to the applied voltage (i.e. returning to the state A). An example of measurements that were taken on a pristine M3M-SBS subjected to 300% biaxial deformation ($\lambda_a = 3$) over one energy generation cycle is shown in Figure 6c, d. Pressure, $P_a(t)$ and volumetric flow of the air in the chamber, $Q_a(t)$, was measured to evaluate the expended mechanical energy per cycle as $W_{mech} = \int P_a(t) dV_a(t)$. Voltage, Φ_L and Φ_H , charging and discharging current, $I_{charge}(t)$ and $I_{discharge}(t)$, on the elastomer were measured to calculate the total converted electric energy as $W_e = (\Phi_H \Phi_L$) $\int I_{charge}(t) dt$ and the generated electric energy as $W_{harvest} = (\Phi_H - \Phi_H) \int I_{charge}(t) dt$ Φ_L) $\int I_{discharge}(t) dt$, followed by evaluation of energy conversion efficiency ratio, η , as $\eta = \frac{W_{harvest}}{W_{mech}}$. A etailed discussion is given in supporting information and Figure 7 shows the states A-D in photos from the harvesting test.

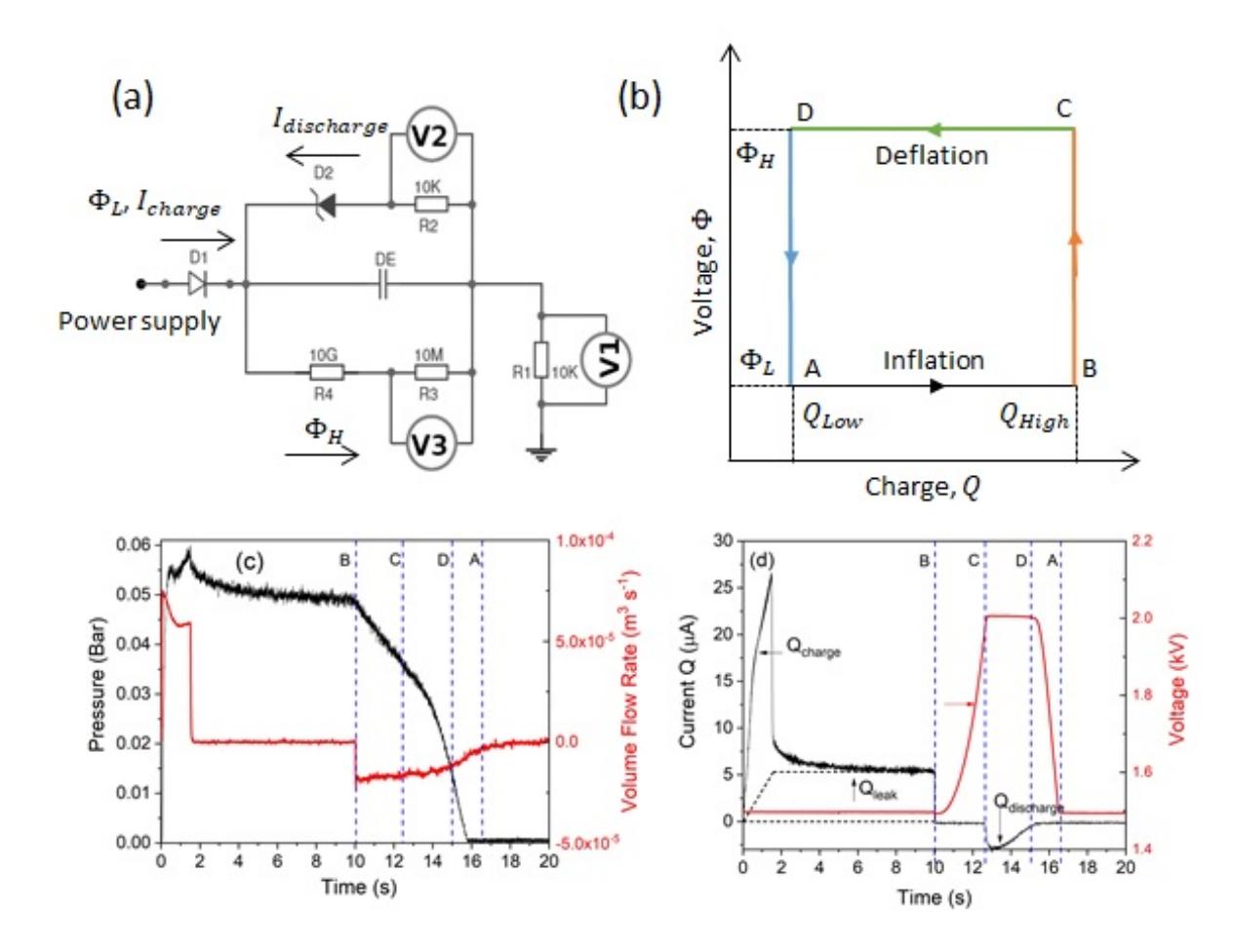


Figure 6 (a) Schematic of energy harvesting cycle for dielectric elastomer (DE) energy generator. (b) Electrical circuit for harvesting and measurements. Voltage input, $\Phi_L = 1.5 \text{ kV}$. Diode D1 allows measurement of harvested voltage at voltmeter V3; D2 is an assembly of Zener diodes in series to establish a constant harvesting voltage of $\Phi_H = 2.0 \text{ kV}$ and allow measurement of the harvested current across a resistor R2 at voltmeter V2. Measurements of M3M-SBS subjected to 300% bi-axial deformation ($\lambda_a = 3$) over one energy generation cycle (20 s): (c) the air pressure, $P_a(t)$ and the volume flow rate, $Q_a(t)$, (d) the voltage, $\Phi(t)$, and the current, air pressure, I(t). The marked states A-D refer to Figure 6b.

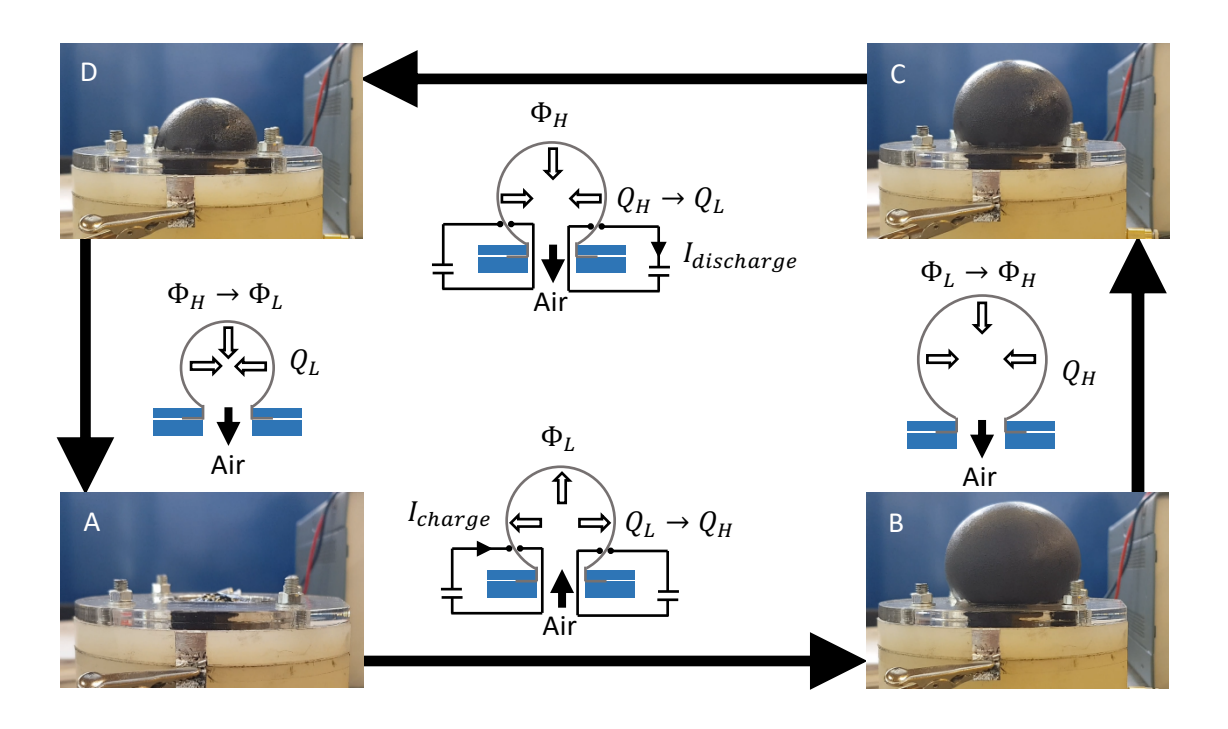


Figure 7 Schematic of energy harvesting cycle with states A-D shown in photos.

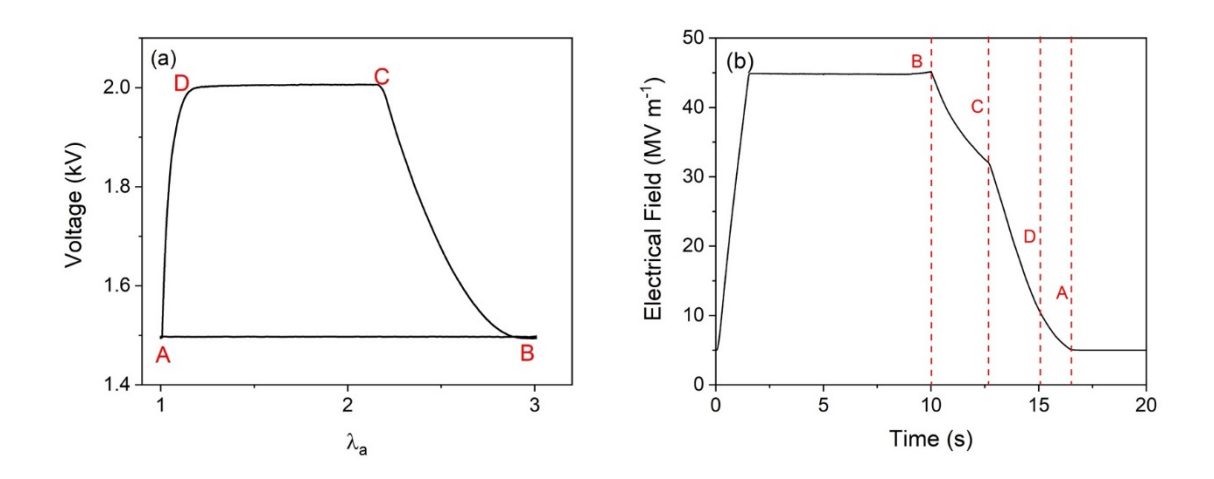


Figure 8 (a) The voltage across the electrodes, against the axial deformation of the elastomer calculated from the volumetric change of the air chamber based on results from Figure 6c. d. (b) Electric field between the electrodes as a function of time with $E_{max} = 45 \text{ MV m}^{-1}$ in the state B. The marked states A-D refer to Figure 6b.

Figure 8a shows the relationship between axial deformation of the elastomer and the voltage across the electrodes. The electric field between the electrodes as a function of time over one energy harvesting cycle was evaluated and is shown in Figure 8b. The maximum electrical field, E_{max} in state B was calculated as $E_{max} = \frac{\phi_L}{H} \lambda_a^2$, to evaluate recoveries in the electrical breakdown strengths of healed elastomers compared with pristine elastomers.

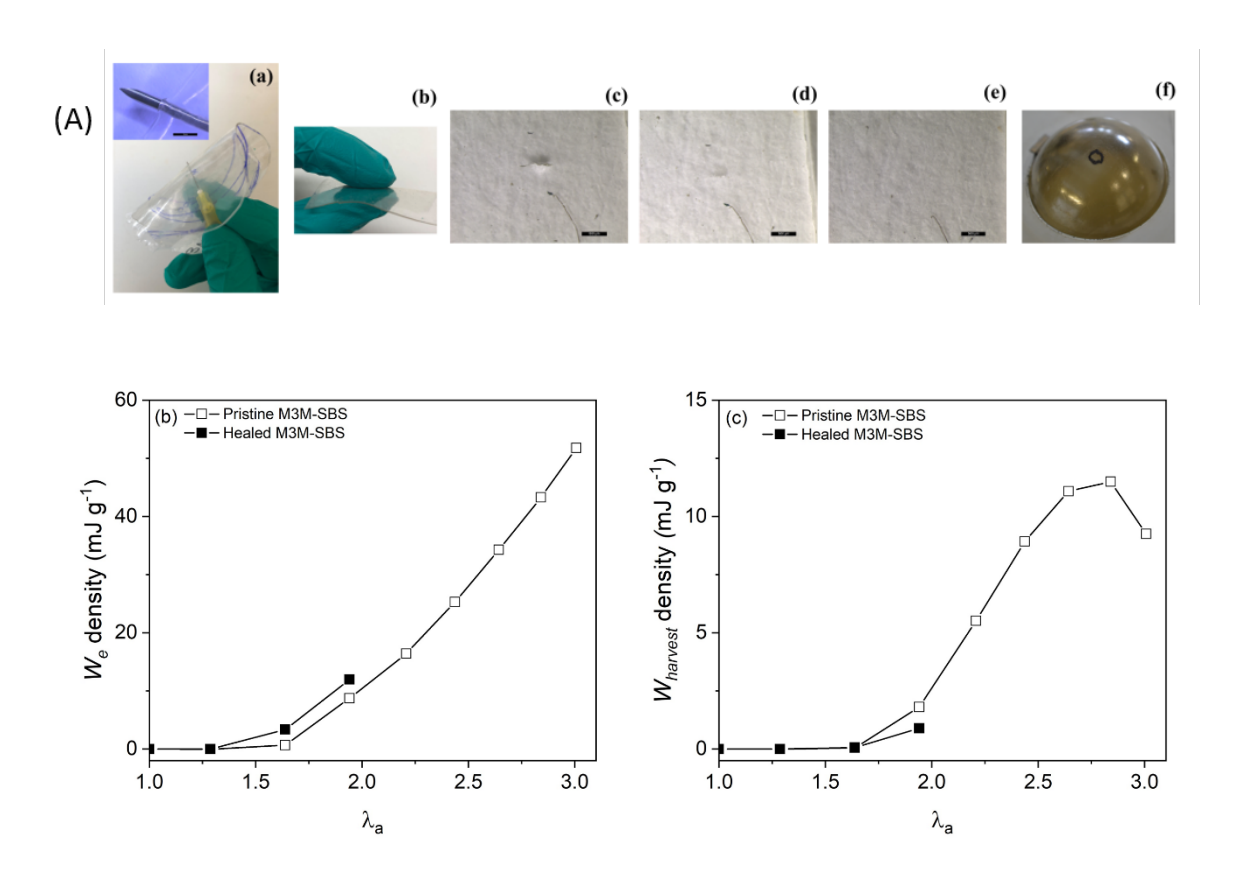


Figure 9 (A) Example of damage introduction and healing of the elastomers. Specific energy of pristine and healed MG-SBS and M3M-SBS per cycle for (B) the total converted electrical energy, W_e and (C) the generated electrical energy, $W_{harvest}$.

Figure 9 (B, C) compares the specific energies that are generated by pristine and healed M3M-SBS that were evaluated from measurements (see also supplementary Figure S6 – S11). Figure 9B shows that, when the energy loss is neglected, both elastomers generate higher specific energy per cycle at larger deformation. At the same electrode region configuration and

deformation, both elastomers generate similar specific energy per cycle for deformations up to $\lambda_a=2.0$. At a larger deformation of $\lambda_a>2.0$, the pristine M3M-SBS generates more specific energy per cycle than healed M3M-SBS as the material fails. Figure 9C shows that in practice, elastomers generated less specific energy per cycle than that in Figure 9B due to energy dissipation. Moreover, it also shows that the generated electrical energy does not always increase with the deformation of the elastomer since current leakage is more severe at larger deformation³¹. The pristine M3M-SBS reached the maxima specific energy per cycle of 11 mJ g⁻¹ at $\lambda_a=2.8$. Note that the performance of a dielectric elastomer generator is also affected by other factors, such as energy harvesting configurations (i.e. harvesting voltage and driving voltage), mechanical loading configurations (i.e. duration of cycle, type of mechanical loading), circuit design and electrode coverage. It is therefore difficult to compare directly the M3M-SBS based energy generators to those in literature. As an approximation in the specific energy per cycle, pristine and healed M3M-SBS are comparable to the commonly used VHB4910, ranging from 2.14 to 400 mJ g⁻¹ ³²⁻³⁴.

Figure 9C also shows that the pristine M3M-SBS was deformed up to $\lambda_a = 3$ with the maximum electric field $E_{max} = 45$ MV m⁻¹ before electric breakdown occurred in the centre; the healed M3M-SBS was deformed up to $\lambda_a = 2$ with $E_{max} = 20$ MV m⁻¹, indicating a recovery in electric breakdown strength of 44%. It is difficult to control the thickness at the healed locality of the elastomer during the self-healing process. Unlike the dielectric elastomer actuator, where planar stresses due to pre-strain were applied at edges of the elastomer, the air pressure was applied equally across the entire elastomer in the dielectric elastomer generator. This means that when the healed locality is thinner than the rest of the film, the air pressure may cause excessive deformation at the healed locality, resulting pre-mature electrical breakdown even when the averaged electrical field across the elastomer is low. This combination of high biaxial strain and high electric field result in the self-healing performance of the dielectric elastomer

generator tend to be lower than that in the dielectric elastomer actuator, which operates at lower strain levels.

Conclusion

We have shown that covalently grafting organic polar groups to elastomers is an effective approach to simultaneously achieve high permittivity, low dielectric loss, high mechanical strain and introduce intermolecular interactions for self-healing to the elastomer.

The polar group methyl-3-mercaptopropionate (M3M) was grafted to SBS via a one-step thiol-ene click chemistry. M3M brings electrostatic interactions between the grafted ester group and styrene group of SBS, and the long side chains benefit chain entanglement. The intrinsic modification lead to a higher permittivity, low loss elastomer with $\epsilon_r \approx 7.5$ and $\tan \delta \approx 0.03$ respectively. Additionally M3M-SBS exhibited an increased strain at break of 1000% and a reduced Young's modulus of 2.4 MPa, increasing the ease of deformation of the material. M3M-SBS demonstrated a more reliable cyclic behaviour over repeated mechanical deformation cycles compared to SBS. The M3M-SBS also showed lower loss per cycle and a lower hysteresis loss overall, retaining 72.3 of its stress after five cycles, compared to 35.2% for SBS. Stress relaxation testing of M3M-SBS demonstrated that the strength of the interchain self-healing interaction present was able to overcome a reduction in chain entanglement in the elastomer after modification, 26 as M3M-SBS retained 65% of its maximum stress, compared to 60% for SBS.

M3M-SBS exhibited the greatest actuation abilities of all three elastomers by axially actuating 9.3% under a 39.6 MV m⁻¹ electrical field. After failure, M3M-SBS had the highest actuation recovery of 85% due to its high strain, low modulus and high breakdown field. Additionally, M3M-SBS had a large material energy density of 11 mJ g⁻¹ during an energy harvesting cycle where $\lambda_a = 2.8$ due to its high electric breakdown strength. This combination

of high biaxial strain and high electric field result in the self-healing performance of the dielectric elastomer generator tend to be lower than that in the dielectric elastomer actuator, which operates at lower strain levels.

This work presents a new generation of intrinsically self-healing elastomers for actuation and energy harvesting, whilst future work should consist of improving the energy harvesting efficiency of the device to better demonstrate the feasible implementation of dielectric energy harvesting devices in everyday life.

Experimental

Materials. Styrene-butadiene-styrene block copolymer (SBS, Vector 8508A) was purchased from Dexco. Tetrahydrofuran (THF, GPR Reactapur, 99.9%), hexane (for HPLC >95%), chloroform-*d* (99.8%), 2,2-dimethoxy-2-phenylacetophenone (DMPA, 99%) and methyl-3-mercaptopropionate (98%) were purchased from Sigma-Aldrich, UK. Carbon black grease was purchased from MG Chemicals, UK to act as a compliant electrode for both actuator and energy harvesting studies.

Synthesis of methyl-3-mercaptopropionate grafted SBS (M3M-SBS). 10 g SBS was dissolved in 90 g of THF. Following this, 0.2 g of DMPA and 145.3 mL (10× molar excess relative to the butadiene block of SBS) of methyl-3-mercaptopropionate was added to the solution. The solution was then irradiated with UV light @ 365 nm with 25% intensity (50 W) using an OmniCure Series 2000 200 W UV lamp for 20 minutes. The resulting modified SBS was purified by precipitation in hexane and dried in a vacuum oven overnight at 60 °C. The mass of the resulting product was 23.7 g (95.2% grafting). 1 H NMR (400 MHz, CDCl₃): δ = 7.08 (br, 3 H, H_{benzene}), 6.54 (br, 2 H, H_{benzene}), 3.72 (S, 3 H, COOCH₃), 2.78 (t, 2 H, SCH₂CH₂, J = 7 Hz), 2.61 (t, 2 H, CH₂CH₂COO, J = 7 Hz) and (br, 1 H, (CH₂)₂CH₃) and (br, 2 H, H₂CCH₂S), 1.75 (br, 2 H, H₂C-CH₂-CH), 1.57 (br, 6 H, (-H₂C)₂CH₂), 1.45 (br, 2 H, -

HCCH₂CH₂), 1.28 (br, 1 H, (H₂C)₃CH) ppm. FT-IR (cm⁻¹): 2928, 1733, 1435, 1243, 1169, 1018, 979, 758.

Characterisation. The elastomers were characterised by ¹H NMR, all spectra were recorded using a Bruker Avance III HD 400 MHz spectrometer. Chemical shifts were internally referenced to TMS using CDCl₃. Spectra were processed using ACD/NMR processor version 12.01 (ACD/Labs). Tensile testing was performed using a Shimadzu Autograph AGS-X tester with samples conforming to ASTM-D638-14 type V. The extension rate was 50 mm min⁻¹ (strain rate = $10.95\% \text{ s}^{-1}$) with a 10 kN load cell and tests were carried out at room temperature. Stress relaxation was investigated by stretching the tensile specimens to 100% elongation at 50 mm min⁻¹ and holding the samples at constant strain until the stress reached equilibrium. This was undertaken to determine the effect of the polar groups grafted and the interactions formed on the relaxation behaviour of the polymer chains. Cyclic stress softening was performed by elongating specimens to strains of 100%, 300% and 500% and back to 0% under a controlled strain rate of 50 mm min⁻¹ for five cycles. The inter-chain interactions of the modified SBS elastomers are studied by using Fourier transform infrared spectroscopy (FT-IR, Bruker Tensor 27 at a resolution of 4 cm⁻¹ with 32 scans), UV-Vis (Agilent Cary 60 photospectrometer, 800 ~ 200 nm) and Dynamic Mechanical Thermal Analysis (DMTA) to support the self-healing mechanism. The DMTA was performed on samples 5.0 mm × 5.0 mm × 2.3 mm in single cantilever mode with a 50 µm amplitude and a frequency of 1 Hz between -120 °C and 135 °C. To measure relative permittivity and loss, impedance spectroscopy measurements were carried out using a Princeton Applied Research Parastat MC with a PMC-2000 card and a two-point probe between $10^{0} \sim 10^{6}$ Hz on thin films of thickness between $100 \sim 200$ µm that were formed by compression moulding using a Rondol manual hot press at 190 °C and 5 kN of force.

Actuation and energy harvesting. To examine the self-healing performance of the actuation and energy harvesting devices, a needle probe (Figure 9a) was employed to inflict mechanical

damage by punching the pristine elastomer in the centre of the electrode region. Finger pressure was applied for 5 minutes, Figure 9a (b), to initiate the healing process, Figure 9a (c). Healed elastomers were then stretched ($\approx 120\%$) and examined to ensure the damage locality remained closed. Finally, healed elastomers were left at room temperature for three days for healing, Figure 9a (d-e), before re-testing in terms of actuation and energy harvesting performance, Figure 9a (f). Self-healing on mechanical damage is meant to assess performances of the material in the ideal case, where contaminations on damaged spots are negligible. Experiments on actuation and energy harvesting were repeated on 3 samples.

To create the dielectric elastomer actuator, both pristine and healed M3M-SBS films with thicknesses of 300 μ m were pre-strained by 33% in planar directions and clamped onto a rigid frame. Conductive carbon grease was applied to form a compliant circular electrode region with a diameter of 15 mm. The applied voltages were increased from 0 to 10 kV to drive actuation, with the voltage-induced planar deformation recorded by a camera. The failure voltage and corresponding electric breakdown strengths of pristine and healed elastomers during actuation were used to evaluate the corresponding dielectric strength recovery.

To evaluate the performance for energy generation, pristine and healed M3M-SBS films with thicknesses of 300 μ m were mounted without pre-strain on the opening of an air chamber with a volume of 55 cm³. Conductive carbon grease was applied to the un-deformed state of the elastomer to form a circular electrode region with the radius of 1.5 cm and re-applied in the deformed states to enhance the electrode coverage. For each energy harvesting cycle of 20 s, the air chamber was pressurized from t=0 s until the target volumetric change was reached. Depressurization occurred from t=10 s until the pressure of the air chamber decreased to atmospheric pressure. The elastomer was inflated and deflated, causing the flat circular region with the radius of 2.25 cm to deform to a near spherical shape with axial deformations from $\lambda = 1.3$ to $\lambda = 3$. Axial deformations of the elastomer were approximated from the volumetric

change of the air chamber, which was confirmed by recorded videos and photography. The failure voltage and corresponding electric breakdown strengths of pristine and healed elastomers were used to evaluate the corresponding level of dielectric strength recovery.

References

- (1) Ellingford, C.; Bowen, C.; McNally, T.; Wan, C. Intrinsically Tuning the Electromechanical Properties of Elastomeric Dielectrics: A Chemistry Perspective. *Macromol. Rapid Commun.* **2018**, *39* (18), 1800340, DOI: 10.1002/marc.201800340.
- (2) Madsen, F. B.; Daugaard, A. E.; Hvilsted, S.; Skov, A. L. The Current State of Silicone-Based Dielectric Elastomer Transducers. *Macromol. Rapid Commun.* **2016**, *37* (5), 378-413, DOI: 10.1002/marc.201500576.
- (3) Kornbluh, R.; Pelrine, R.; Prahlad, H.; Wong-Foy, A.; McCoy, B.; Kim, S.; Eckerle, J.; Low, T. Dielectric elastomers: Stretching the Capabilities of Energy Harvesting. *MRS Bull*. **2012**, *37* (03), 246-253.
- (4) Rehman, H. U.; Chen, Y.; Hedenqvist, M. S.; Pathan, R.; Liu, H.; Wang, H.; Chen, T.; Zhang, X.; Li, H. High-Cycle-Life and High-Loading Copolymer Network with Potential Application as a Soft Actuator. *Materials & Design* **2019**, *182*, 108010, DOI: https://doi.org/10.1016/j.matdes.2019.108010.
- (5) Khan, N. I.; Halder, S.; Gunjan, S. B.; Prasad, T. A Review on Diels-Alder Based Selfhealing Polymer Composites. *IOP Conference Series: Materials Science and Engineering* **2018**, *377*, 012007, DOI: 10.1088/1757-899x/377/1/012007.
- (6) Liu, Y.-L.; Chuo, T.-W. Self-healing Polymers Based on Thermally Reversible Diels–Alder Chemistry. *Polym. Chem.* **2013**, *4* (7), 2194-2205, DOI: 10.1039/C2PY20957H.
- (7) Bai, J.; Li, H.; Shi, Z.; Tian, M.; Yin, J. Dynamic Crosslinked Poly(styrene-block-butadiene-block-styrene) via Diels-Alder Chemistry: an Ideal Method to Improve Solvent Resistance and Mechanical Properties Without Losing its Thermal Plastic Behavior. *RSC Adv.* **2015**, *5* (56), 45376-45383, DOI: 10.1039/C5RA08719H.
- (8) Zhang, L.; Qiu, T.; Zhu, Z.; Guo, L.; Li, X. Self-Healing Polycaprolactone Networks through Thermo-Induced Reversible Disulfide Bond Formation. *Macromol. Rapid Commun.* **2018**, *39* (20), 1800121, DOI: 10.1002/marc.201800121.

- (9) Ling, L.; Li, J.; Zhang, G.; Sun, R.; Wong, C.-P. Self-Healing and Shape Memory Linear Polyurethane Based on Disulfide Linkages with Excellent Mechanical Property. *Macromol. Res.* **2018**, *26* (4), 365-373, DOI: 10.1007/s13233-018-6037-9.
- (10) Lee, S.-H.; Shin, S.-R.; Lee, D.-S. Self-healing of Cross-linked PU via Dual-Dynamic Covalent Bonds of a Schiff Base from Cystine and Vanillin. *Materials & Design* **2019**, *172*, 107774, DOI: https://doi.org/10.1016/j.matdes.2019.107774.
- (11) Mo, R.; Hu, J.; Huang, H.; Sheng, X.; Zhang, X. Tunable, Self-healing and Corrosion Inhibiting Dynamic Epoxy–Polyimine Network Built by Post-Crosslinking. *J. Mater. Chem. A* **2019**, *7* (7), 3031-3038, DOI: 10.1039/C8TA11546J.
- (12) Pan, Y.; Hu, J.; Yang, Z.; Tan, L. From Fragile Plastic to Room-Temperature Self-Healing Elastomer: Tuning Quadruple Hydrogen Bonding Interaction through One-Pot Synthesis. *ACS Applied Polymer Materials* **2019**, *I* (3), 425-436, DOI: 10.1021/acsapm.8b00153.
- (13) Fan, C.-J.; Huang, Z.-C.; Li, B.; Xiao, W.-X.; Zheng, E.; Yang, K.-K.; Wang, Y.-Z. A Robust Self-healing Polyurethane Elastomer: From H-bonds and Stacking Interactions to Well-Defined Microphase Morphology. *Science China Materials* **2019**, *62* (8), 1188-1198, DOI: 10.1007/s40843-019-9422-7.
- (14) Chen, J.; Li, F.; Luo, Y.; Shi, Y.; Ma, X.; Zhang, M.; Boukhvalov, D. W.; Luo, Z. A Selfhealing Elastomer Based on an Intrinsic Non-Covalent Cross-linking Mechanism. *J. Mater. Chem. A* **2019**, *7* (25), 15207-15214, DOI: 10.1039/C9TA03775F.
- (15) Das, A.; Sallat, A.; Böhme, F.; Suckow, M.; Basu, D.; Wießner, S.; Stöckelhuber, K. W.; Voit, B.; Heinrich, G. Ionic Modification Turns Commercial Rubber into a Self-Healing Material. *ACS Appl. Mater. Interfaces* **2015,** *7* (37), 20623-20630, DOI: 10.1021/acsami.5b05041.
- (16) Mei, J.-F.; Jia, X.-Y.; Lai, J.-C.; Sun, Y.; Li, C.-H.; Wu, J.-H.; Cao, Y.; You, X.-Z.; Bao, Z. A Highly Stretchable and Autonomous Self-Healing Polymer Based on Combination of Pt···Pt and π – π Interactions. *Macromol. Rapid Commun.* **2016**, *37* (20), 1667-1675, DOI: 10.1002/marc.201600428.
- (17) Liu, L.; Yan, S.; Zhang, L. A Self-Healing Dielectric Supramolecular Elastomer Functionalized with Aniline Tetramer. *Macromol. Rapid Commun.* **2018**, *39* (20), 1800349, DOI: 10.1002/marc.201800349.
- (18) Du, L.; Xu, Z.-Y.; Fan, C.-J.; Xiang, G.; Yang, K.-K.; Wang, Y.-Z. A Fascinating Metallo-Supramolecular Polymer Network with Thermal/Magnetic/Light-Responsive Shape-Memory Effects Anchored by Fe3O4 Nanoparticles. *Macromolecules* **2018**, *51* (3), 705-715, DOI: 10.1021/acs.macromol.7b02641.

- (19) Zheng, Q.; Ma, Z.; Gong, S. Multi-Stimuli-Responsive Self-healing Metallo-Supramolecular Polymer Nanocomposites. *J. Mater. Chem. A* **2016**, *4* (9), 3324-3334, DOI: 10.1039/C5TA10694J.
- (20) Campanella, A.; Döhler, D.; Binder, W. H. Self-Healing in Supramolecular Polymers. *Macromol. Rapid Commun.* **2018**, *39* (17), 1700739, DOI: 10.1002/marc.201700739.
- (21) Sun, H.; Liu, X.; Liu, S.; Yu, B.; Ning, N.; Tian, M.; Zhang, L. Silicone Dielectric Elastomer with Improved Actuated Strain at Low Electric Field and High Self-healing Efficiency by Constructing Supramolecular Network. *Chem. Eng. J.* **2020**, *384*, 123242, DOI: https://doi.org/10.1016/j.cej.2019.123242.
- (22) Madsen, F. B.; Yu, L.; Skov, A. L. Self-Healing, High-Permittivity Silicone Dielectric Elastomer. *ACS Macro Letters* **2016**, *5* (11), 1196-1200, DOI: 10.1021/acsmacrolett.6b00662.
- (23) Dunki, S. J.; Cuervo-Reyes, E.; Opris, D. M. A Facile Synthetic Strategy to Polysiloxanes Containing Sulfonyl Side Groups with High Dielectric Permittivity. *Polym. Chem.* **2017**, *8* (4), 715-724, DOI: 10.1039/C6PY01917J.
- (24) Racles, C.; Alexandru, M.; Bele, A.; Musteata, V. E.; Cazacu, M.; Opris, D. M. Chemical Modification of Polysiloxanes with Polar Pendant Groups by Co-Hydrosilylation. *RSC Adv.* **2014**, *4* (71), 37620-37628, DOI: 10.1039/C4RA06955B.
- (25) Huang, C.; Zhang, Q. M. Fully Functionalized High-Dielectric-Constant Nanophase Polymers with High Electromechanical Response. *Adv. Mater.* **2005**, *17* (9), 1153-1158, DOI: 10.1002/adma.200401161.
- (26) Ellingford, C.; Zhang, R.; Wemyss, A. M.; Bowen, C.; McNally, T.; Figiel, Ł.; Wan, C. Intrinsic Tuning of Poly(styrene–butadiene–styrene)-Based Self-Healing Dielectric Elastomer Actuators with Enhanced Electromechanical Properties. *ACS Appl. Mater. Interfaces* **2018**, *10* (44), 38438-38448, DOI: 10.1021/acsami.8b13785.
- (27) Zhang, Y.; Ellingford, C.; Zhang, R.; Roscow, J.; Hopkins, M.; Keogh, P.; McNally, T.; Bowen, C.; Wan, C. Electrical and Mechanical Self-Healing in High-Performance Dielectric Elastomer Actuator Materials. *Adv. Funct. Mater.* **2019**, *29* (15), 1808431, DOI: 10.1002/adfm.201808431.
- (28) Tian, M.; Yan, H.; Sun, H.; Zhang, L.; Ning, N. Largely Improved Electromechanical Properties of Thermoplastic Dielectric Elastomers by Grafting Carboxyl onto SBS Through Thiol-ene Click Chemistry. *RSC Adv.* **2016**, *6* (98), 96190-96195, DOI: 10.1039/C6RA17871E.
- (29) Perju, E.; Ko, Y. S.; Dünki, S. J.; Opris, D. M. Increased Electromechanical Sensitivity of Polysiloxane Elastomers by Chemical Modification with Thioacetic Groups. *Materials & Design* **2020**, *186*, 108319, DOI: https://doi.org/10.1016/j.matdes.2019.108319.

- (30) Sheima, Y.; Caspari, P.; Opris, D. M. Artificial Muscles: Dielectric Elastomers Responsive to Low Voltages. *Macromol. Rapid Commun.* **2019**, *40* (16), DOI: 10.1002/marc.201900205.
- (31) Chiang Foo, C.; Cai, S.; Jin Adrian Koh, S.; Bauer, S.; Suo, Z. Model of Dissipative Dielectric Elastomers. *J. Appl. Phys.* **2012**, *111* (3), 034102, DOI: 10.1063/1.3680878.
- (32) Pelrine, R.; Kornbluh, R. D.; Eckerle, J.; Jeuck, P.; Oh, S.; Pei, Q.; Stanford, S. In *Dielectric elastomers: Generator Mode Fundamentals and Applications*, SPIE's 8th Annual International Symposium on Smart Structures and Materials, SPIE: 2001; p 9.
- (33) Jean-Mistral, C.; Basrour, S.; Chaillout, J.-J., Dielectric Polymer: Scavenging Energy from Human Motion. In *SPIE Smart Structures and Materials + Nondestructive Evaluation and Health Monitoring*, SPIE: 2008; Vol. 6927, p 10.
- (34) Graf, C.; Maas, J. Evaluation and Optimization of Energy Harvesting Cycles Using Dielectric Elastomers, SPIE: 2011; Vol. 7976.

Acknowledgement

CE thanks EPSRC and Jaguar Land Rover (UK) for funding this PhD studentship.

Additional Information

The authors declare no competing interests

Supporting Information

Figure S1 Chemical modification of SBS to form M3M-SBS.

Figure S2 Cyclic stress softening of SBS and M3M-SBS for 100% and 300% strain, first cycle and fifth cycle.

Figure S3 AC conductivity of SBS and M3M-SBS between $10^0 - 10^6$ Hz

Figure S4 (a) Healed strain at break, (b) strain at break recovery and (c) stress-strain curves for M3M-SBS at different time steps at room temperature

Figure S5 Temperature dependent FTIR for SBS (a) at 1730 cm⁻¹, (b) at 1356 cm⁻¹ and (c) at 1243 cm⁻¹

Figure S6 Measured energy harvesting cycles for M3M-SBS with the total deformation of $\lambda_a = 3$, in: (a) mechanical and (b) electrical work-conjugate plane. The enclosed areas by the contours correspond to (a) the expended mechanical energy, W_{mech} , of [178 mJ (324 mJ g⁻¹)] and (b) the total converted electrical energy, W_e , of [13 mJ (52 mJ g⁻¹)] and the actual harvested electrical energy, $W_{harvest}$, of [2.3 mJ (9.2 mJ g⁻¹)]. The marked states A-D refer to Figure 6b.

Figure S7 Measurements of (a) air pressure and (b) volumetric flow rates for the pristine M3M-SBS in energy harvesting test.

Figure S8 Measurements of (a) the voltage across the electrodes, (b) the charging current and (c) the discharging current for the pristine M3M-SBS in energy harvesting test.

Figure S9 Measurements of (a) air pressure and (b) volumetric flow rates for the healed M3M-SBS in energy harvesting test.

Figure S10 Measurements of (a) the voltage across the electrodes, (b) the charging current and (c) the discharging current for the healed M3M-SBS in energy harvesting test.

Figure S11 The actual energy conversion efficiency of pristine and healed M3M-SBS.